Crystal Structure and Enantiomer Selection by D-Alanyl Carrier Protein Ligase DltA from *Bacillus cereus*[†]

Liqin Du, Yujiong He, and Yu Luo*

Department of Biochemistry, University of Saskatchewan, A3 Health Sciences Building, 107 Wiggins Road, Saskatoon, Saskatchewan, Canada S7N 5E5

Received July 21, 2008; Revised Manuscript Received September 12, 2008

ABSTRACT: Ubiquitous D-alanylation of lipoteichoic acids modulates the surface charge and ligand binding of the Gram-positive cell wall. Disruption of the bacterial *DltABCD* gene involved in teichoic acid alanylation, as well as inhibition of the DltA protein, has been shown to increase a Gram-positive bacterium's susceptibility to antibiotics. The DltA D-alanyl carrier protein ligase promotes a two-step process starting with adenylation of D-alanine. We have determined the 2.0 Å resolution crystal structure of a DltA protein from *Bacillus cereus* in complex with the D-alanine adenylate intermediate of the first reaction. Despite the low level of sequence similarity, the DltA structure resembles known structures of adenylation domains such as the acetyl-CoA synthetase. The enantiomer selection appears to be enhanced by the medium-sized side chain of Cys-269. The Ala-269 mutant protein shows marked loss of such selection. The network of noncovalent interactions between the D-alanine adenylate and DltA provides structure-based rationale for aiding the design of tight-binding DltA inhibitors for combating infectious Gram-positive bacteria such as the notorious methicillin-resistant *Staphylococcus aureus*.

Cell walls of most studied Gram-positive bacteria contain teichoic acids, polymers of glycerol phosphate, or ribitol phosphate. These polymers are covalently linked to either peptidoglycan (wall teichoic acids) or glycolipids (lipoteichoic acids). The remaining hydroxyls of this anionic polymer are ubiquitously modified by D-alanyl esterification or glycosylation (*1*−*3*). In studied bacteria, a *dlt* operon, which typically codes for DltA,[1] DltB, DltC, and DltD proteins, is responsible for the D-alanylation of teichoic acids (*4*). Alanylation reduces the net charge on the polymer. At least four possible functions of the D-alanylated teichoic acids have been proposed (*5*): (i) regulation of autolysins (*3*); (ii) cation homeostasis; (iii) trafficking of nutrients, proteins, and antibiotics; and (iv) presentation of envelope proteins. The *dlt* gene appears to be unnecessary for survival and growth of Gram-positive bacteria in the absence of stress (*6*). However, reduced D-alanyl content of the cell wall enhances autolysis (*3, 6*) and renders the bacteria susceptible to host defense peptides and other antibiotics (*7, 8*). In addition, lack of D-alanylation of teichoic acid impairs the ability of Gram-positive bacteria to colonize (*9*) and form antibiotic-resistant biofilms (*10*). Therefore, the teichoic acid D-alanylation pathway could serve as a novel target for combating emerging infectious diseases caused by Gram-positive bacteria such as the methicillin-resistant *Staphylococcus aureus* (*5*).

The D-alanyl carrier protein ligase DltA (~500 amino acid residues) (*4*) is an enzyme resembling the adenylation domains (also called AMP-forming domains) found in modular nonribosomal peptide synthetases (*11*). Its remote homologues include the acetyl-CoA synthetases and firefly luciferases (*12*). As illustrated in Figure 1A, DltA catalyzes the ATP-driven adenylation of D-alanine and the transfer of the activated D-alanyl to the thiol group of 4′-phosphopantetheine which is covalently attached to a serine side chain of D-alanyl carrier protein DltC (~80 amino acid residues) (*4*). The roles have not been firmly established for DltB, an integral membrane protein, and DltD, a protein bound to the membrane via an N-terminal transmembrane domain. Possibly, these two proteins facilitate the transport of DltC-linked D-alanyl across the cell membrane and alanylation of teichoic acid (*13*).

DltA, as the first confirmed enzyme in the teichoic acid D-alanylation pathway, stands out as a potential antimicrobial target. The first characterized DltA inhibitor 5′-*O*-[*N*-(D-alanyl)-sulfamoyl]adenosine, an analogue of D-alanyl adenylate, significantly suppressed the growth of *Bacillus subtilis* when used in combination with vancomycin (*14*). Uniquely, this protein appears to directly activate D-alanine rather than depending on an epimerization domain which converts an activated L-amino acid into the corresponding D-form (*14*). In order to rationalize its substrate selection mechanism as well as provide a structural basis for inhibitor design, we have determined the crystal structure of DltA from *Bacillus cereus* and studied its preference of D-alanine over L-alanine.

[†] This work is supported by a Saskatchewan Health Research Foundation grant to the Molecular Design Research Group at University of Saskatchewan and by Canadian Institute of Health Research Operating Grant 63860 to Y.L.

* Corresponding author. Telephone: 306-9664379. Fax: 306-966-4390. E-mail: yu.luo@usask.ca.

[1] Abbreviations: DltA, D-alanine carrier protein ligase; BcDltA, D-alanine carrier protein ligase from *Bacillus cereus*; PheA, phenylalanine-activating domain of the first module of the *Bacillus brevis* gramicidin S synthetase I; DhbE, 2,3-dihydroxybenzoate activation domain from *B. subtilis*; ACS, acetyl-CoA synthetase; DltC, D-alanine carrier protein; ATP, adenosine 5′-triphosphate; AMP, adenosine 5′-monophosphate; IPTG, isopropyl β-D-1-thiogalactopyranoside.

10.1021/bi801363b CCC: $40.75
Published on Web 10/11/2008

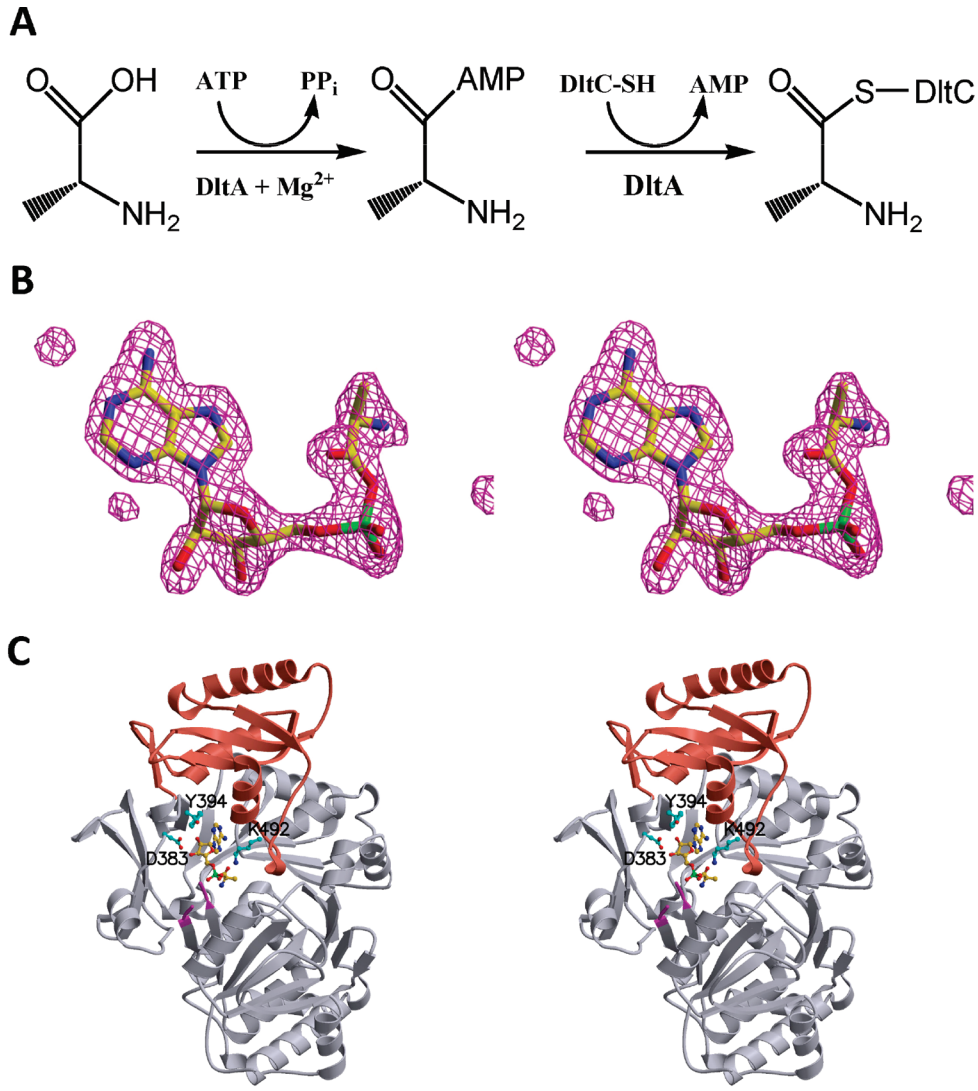

FIGURE 1: Structure and function of DltA. (A) Two-step reaction catalyzed by DltA. In the first step, D-alanine is converted into DltA-bound D-alanine adenylate (D-Ala-AMP). In the second step, the activated D-alanyl is transferred to the thiol group of DltC-linked 4′-phosphopantetheine (HS-DltC). (B) The omit $F_o - F_c$ difference maps (in magenta) were contoured at 4σ after simulated annealing starting at 2000 K. The D-alanine adenylate is shown in sticks with C, O, N, and P atoms in yellow, red, blue, and green, respectively. (C) The major and minor domains of BcDltA are shown in gray and salmon, respectively. The bound D-alanine adenylate and side chains of Asp-383, Tyr-394, and Lys-492 are shown in sticks. The C atoms in the side chains are shown in cyan. The anchoring residues (152−153 and 159−160) of the disordered loop (154−158) are highlighted in magenta.

EXPERIMENTAL PROCEDURES

Cloning, Protein Preparation, and Crystallization. The chemicals were purchased from VWR unless specified otherwise. The open reading frame of DltA from *B. cereus* was amplified by polymerase chain reaction using *Pfu* DNA polymerase (Fermentas) from genomic DNA (American Type Culture Collection). Two oligonucleotide primers (BcDltANcoIFor, CATG*CCATGG*CAAAG TTATT AGAAC AAATT GAAA AGTGG G, and BcDltAXhoIRev, CCG CTCGAG TGCTG TAACC TCACT CA) were purchased from Integrated DNA Technologies. The amplified DNA and pET28a plasmid (Novagen) were both digested using *Nco*I and *Xho*I restriction enzymes and ligated using T4 DNA ligase (New England Biolabs). Electrocompetent XL-1 Blue cells (Stratagene) were transformed and selected by plating on LB/agar media with 35 mg/L kanamycin. Plasmids with the DltA insert were purified using a plasmid purification kit (QIAGEN). The pET28a-BcDltA construct carries an Ala-1 mutation at the N-terminus and eight extra residues at the C-terminus (LEHHHHHH). After verification by DNA sequencing, the construct was used to transform electrocompetent BL21-Rosetta2 (DE3) cells (Novagen). The expression of recombinant DltA was induced with 0.5 mM IPTG when 1 L of cell culture in the presence of 35 mg/L kanamycin and 35 mg/L chloramphenicol at 37 °C reached an optical density of 0.5−0.8 at 600 nm. Cells were cooled down to 25 °C and harvested ~16 h after IPTG induction by centrifugation at 5000*g*. The cell pellet was frozen at −20 °C overnight and thawed in 100 mL of nickel-binding buffer (0.5 M NaCl and 30 mM Tris-HCl at pH 7.9) before cell lysis by sonication. The insoluble debris was removed by centrifugation at 20000*g*, and the supernatant was loaded onto a 10 mL column packed with His-select nickel affinity gel (Sigma-Aldrich). The column was washed with 150 mL of wash buffer (0.5 M NaCl, 30 mM imidazole-HCl at pH 7.5). The column-bound proteins were eluted by 0.5 M NaCl and 20 mM EDTA−Tris at pH 7.5. The eluted proteins were precipitated by adding 0.3 g/mL ammonium sulfate and

stored at 4 °C overnight. The protein precipitate was collected by centrifugation at 20000*g* and redissolved in 10 mL of gel filtration buffer (0.2 M NaCl, 0.02 M Tris-HCl at pH 7.4). The gel filtration purification was performed using a HiPrep Sephacryl S-300 column (GE Health Science), and the fractions containing BcDltA were concentrated to at least 20 mg/mL by ultrafiltration. The C269A mutation was introduced by following the one-step site-directed mutagenesis protocol (*15*) using the pET28a-BcDltA construct as the template for amplification using *Pfu* DNA polymerase and a pair of mutagenic pimers (C269AFor, CATTC TTATT CGCCG GTGAA GTGTT ACCAA ATGAA G, and C269ARev, CACTT CACCG GCGAA TAAGA ATGTT TTCAT GTTCG). The mutant C269A protein was purified following the same procedure for the wild-type protein.

Crystallization and Structure Determination. The concentrated BcDltA protein (20−30 mg/mL) was crystallized using the hanging drop crystallization method at a room temperature of 21 °C. The protein was premixed with 1 mM ATP and 1 mM D-alanine (both from Sigma-Aldrich). The optimal well solution for crystallization contained 0.1 M $MgCl_2$, 0.2 M KCl, 12% PEG 3350 (Sigma-Aldrich), and 0.05 M Hepes−NaOH buffer at pH 7.2. Each drop was composed of 1 μL of protein and 1 μL of well solution. The plate-shaped crystals grew to a maximal size of 0.5 mm wide and 0.05 mm thick in 2 days. Crystals were gradually transferred to soaking solutions composed of the crystallization reservoir solution supplemented with 5%, 10% 15%, 20%, and 25% glycerol and 1 mM fresh ATP and D-alanine, soaked for 2 min, and then flash-cooled to 100 K in a nitrogen stream generated by an Oxford CryoSystems device. The 0.4° oscillation images were acquired and processed using a Brukers Proteum-R system as described (*16*). The previously solved PheA model (PDB code 1AMU) (*17*) retrieved from the Protein Data Bank (*18, 19*) was used as the model for molecular replacement solution using AMoRe (*20*). The resulting model and electron density map were improved by Arp/Warp (*21*). The model was iteratively rebuilt using XtalView (*22*) and refined using CNS (*23*). A 3.0 Å resolution anomalous difference map was generated using model-derived phases retarded by 90°. Peaks in this anomalous difference map were used as guides for sulfur atoms in Cys and Met residues. The bound D-alanine adenylate was modeled using the difference electron density map. The final model has 91.1% of the residues in the most favored regions on a Ramachandran plot. Val-301 is the only residue found in the disfavored region. This residue lies in a region with clear electron density. Statistics of the diffraction data, refinement, and geometry are listed in Table 1. The molecular figures were generated using Molscript (*24*) and rendered using Raster3D (*25*). The coordinates and structure factors have been deposited in the Protein Data Bank (entry code 3DHV).

Pyrophosphate Detection Assay. A dye solution containing 0.033% (w/v) Malachite Green, 1.3% (w/v) ammonium molybdate, and 1.0 M HCl was used to monitor the release of inorganic phosphate (*26*) from a pyrophosphatase-coupled reaction. Absorbance at 620 nm was recorded for quantification. The 200 μL reaction solutions contained 5 μM BcDltA, 5 mM ATP, 0.1 M KCl, 0.01 M $MgCl_2$, 0.05 M Tris−Hepes buffer at pH 7.4, 5 units/mL inorganic pyrophosphatase from baker's yeast (Sigma-Aldrich), and the specified concentration of alanine (Sigma-Aldrich). Concentrated BcDltA was added after a preincubation step at 37 °C for at least 5 min to remove any potential pyrophosphate contamination. A volume of 25 μL of reaction solution was retrieved every 5 min and immediately mixed with 475 μL of the dye solution. The absorption at 620 nm was recorded after 90 s. The initial rates (half of the inorganic phosphate accumulation per minute) of the reaction were derived from the time courses of phosphate accumulation. The trend of rate against alanine concentration was fitted with a hyperbola using the Prism software (GraphPad Software).

Table 1: X-ray Crystallographic Data Collection and Structure Refinement Statistics

	BcDltA/D-alanine adenylate complex
Data Collection	
space group	$P2_1$
cell dimensions	
a, *b*, *c* (Å)	60.7, 86.7, 57.4
α, *β*, *γ* (deg)	90.0, 113.5, 90.0
resolution (Å)	2.0 (2.09−2.00)[a]
R_{sym}	0.074 (0.265)
$I/\sigma I$	8.0 (1.9)
no.of reflections	35392 (3576)
completeness (%)	95.7 (76.2)
redundancy	5.15 (3.6)
Refinement	
resolution (Å)	20.0−2.0
no. of reflections	35313
R_{work}/R_{free}	0.217/0.258
no. of atoms	
protein	3934
ligand/ion	28
water	197
average *B*-factors (Å^2)	
protein	22.5
ligand	12.3
water	27.6
rms deviations	
bond lengths (Å)	0.006
bond angles (deg)	1.26

[a] Values in parentheses refer to values in the highest resolution shell. [b] $R_{sym} = \sum|I_h - \langle I\rangle_h|/\sum I_h$, where $\langle I\rangle_h$ is average intensity over symmetry equivalents and h is the reflection index. [c] $R_{work} = \sum|F_c - F_o|/\sum F_o$. The summation is over all reflections used in refinement. R_{free} is calculated using a randomly selected 5% of the reflections set aside throughout the refinement.

RESULTS

Overall Structure of BcDltA in Complex with D-Alanine Adenylate. DltA protein from *B. cereus* was crystallized in the presence of ATP, D-alanine, and magnesium. One crystal diffracted to 2.0 Å resolution (Table 1). The electron density map (Figure 1B) indicated the presence of a bound D-alanine adenylate, the product of the first reaction step catalyzed by DltA proteins (Figure 1A). Except for residues 154−158, the polypeptide chain is highly ordered. The disordered segment belongs to a highly conserved region shown to be important for the adenylation step in homologous proteins (*27*−*29*). Due to its similar amino acid composition (glycine, serine, threonine, and lysine) to that of the P-loop in ATPases and GTPases (*30*), this loop was hypothesized to be involved in ATP or pyrophosphate binding. The disordered state of this loop, as observed in most homologous structures, also implies a possibility of its involvement in binding ATP or

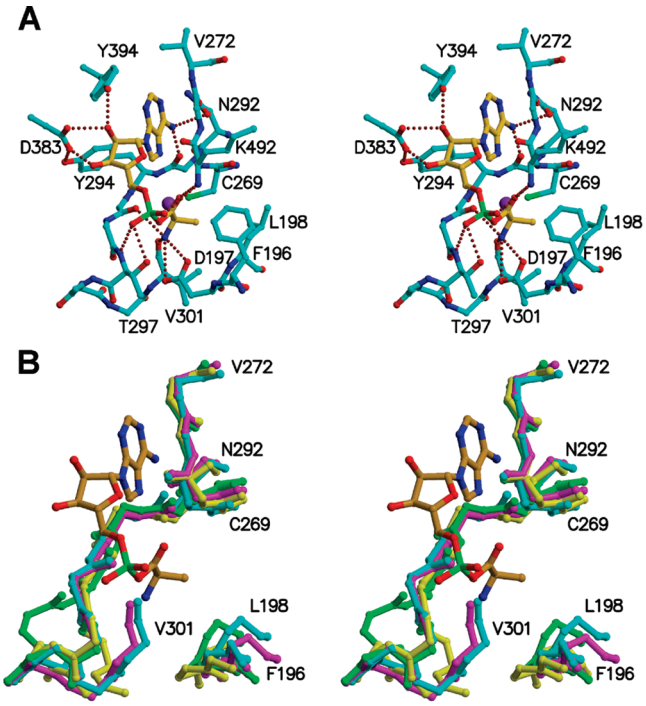

FIGURE 2: Structure of the active site in stereo. The orientation is similar to that in Figure 1B,C. (A) Ball-and-stick model of the active site. The atom coloring scheme is similar to that in Figure 1. The Sγ atom in Cys-269 is shown in green. The modeled C$_\beta$ atom of L-alanine is highlighted in purple. Selected hydrogen bonds are shown in brown dashed lines. (B) Comparison of substrate-binding pockets in DltA homologues. The D-alanine adenylate is colored as in panel A. Three main chain segments of BcDltA (in cyan), PheA (in magenta), DhbE (in green), and yeast ACS (in yellow) are shown. The three homologous structures, PheA (in complex with AMP and phenylalanine, PDB code 1AMU), DhbE (in complex with the adenylate intermediate, PDB code 1MDB), and yeast ACS (in complex with AMP, PDB code 1RY2), have also been crystallized in their respective adenylation conformation. The starting and ending residues of BcDltA are labeled. The substrate-binding pocket is lined by residues around Leu-198, Cys-269, and Val-301.

pyrophosphate. Although ordered states of equivalent loops have been observed in at least two homologues (*31, 32*), there have been no structural data for such an adenylation domain in complex with ATP or pyrophosphate to verify this assumption. The 504-residue BcDltA structure can be approximately divided into two domains (Figure 1C): an N-terminal major domain from the N-terminus to residue 399, and a C-terminal minor domain from residue 400 to the C-terminus.

D-Alanine Adenylate-Binding Pocket. The adenylate was observed in the interface between the two domains. Three segments (Phe-196 to Leu-198, Cys-269 to Val-272, and Asn-292 to Val-301) partially enclose the D-alanine adenylate intermediate (Figure 2A). Three additional side chains (Asp-383, Tyr-394, and Lys-492) participate in close contacts with the adenylate. The adenine moiety is intercalated by unusually flat peptide planes between Gly-270 and Val-272 on one side and the aromatic side chain of Tyr-294 on the opposite side. The 6-amino group forms hydrogen bonds with the side chain carbonyl oxygen of Asn-292 and the main chain oxygen of Thr-293. The ribose appears anchored by two hydrogen bonds between its 2′- and 3′-hydroxyls and the carboxylate group of Asp-383. The 2′-hydroxyl also forms a hydrogen bond with the Tyr-394 side chain. The α-phosphate forms hydrogen bonds with the β-hydroxyl and amide groups of Thr-297 and the ε-amino group of Lys-492. The lysyl residue also forms a hydrogen bond with the D-alanyl carbonyl oxygen. The rest of the D-alanine-binding pocket is lined by residues Phe-196 to Leu-198, Cys-269 to Gly-270, Gly-295 to Pro-296, and Val-301. The D-alanyl amino group forms hydrogen bonds with the carboxylate group of Asp-197 and with the main chain carbonyl oxygen atoms of Gly-295 and Val-301. The D-alanyl methyl group points toward Leu-198. The sulfur atom of Cys-269 is positioned 3.6 Å from the α-carbon of the D-alanyl moiety. A modeled L-alanine positions its α-methyl group (purple sphere, Figure 2A) as close as 2.6 Å to the side chain thiol group of Cys-269. Such a close encounter would result in steric clashes and disfavor the binding of L-alanine.

Comparison with Known Structures of Homologous AMP-Forming Domains. The BcDltA structure appeared to be most similar to PheA (*17*) based on comparison with known structures using the ProFunc server (*33*). A root-mean-square deviation of 1.91 Å was obtained between 406 Cα atoms in 38 equivalent secondary structure elements of BcDltA and PheA. Less than 34 equivalent secondary structure elements were found between BcDltA and other known structures with root-mean-square deviations greater than 2.4 Å. Despite high level of variation in their amino acid sequences among homologous adenylation proteins, all known structures of such domains appear to share a relatively conserved major N-terminal domain and a minor C-terminal domain. Two drastically different dispositions of the two domains have been observed in homologous structures. The first is apparently relevant to the adenylation reaction, in which the minor domain contributes a lysyl side chain (Lys-492 in BcDltA) which bridges the nucleophilic attack of a carboxylate group on the α-phosphate of ATP (*34*). The other is thought to be relevant to the transfer reaction of the adenylated intermediate to the thiol group of coenzyme A or the 4′-phosphopantetheine group of a carrier protein (*31, 32*). This structure of BcDltA appears to be determined in a conformation relevant to the adenylation reaction. In order to analyze the substrate selection, we compared the BcDltA structure with three homologous structures of this enzyme superfamily determined in their respective adenylation conformation: PheA (phenylalanine-activating domain of the first module of the *Bacillus brevis* gramicidin S synthetase I, in complex with AMP and phenylalanine, PDB code 1AMU) (*17*), DhbE (2,3-dihydroxybenzoate activation domain from *B. subtilis*, in complex with the adenylate intermediate, PDB code 1MDB) (*35*), and yeast ACS (acetyl-CoA synthetase, in complex with AMP, PDB code 1RY2) (*36*). In addition to the conserved Lys residue, the ribose-anchoring Asp (residue 383 in BcDltA) is conserved, and the adenine-interacting Tyr (residue 294 in BcDltA) is somewhat conserved as a Tyr or Phe. The adenosine-wrapping main chain segments corresponding to Gly-270 to Val-272 and Asn-292 to Ala-299 of BcDltA appear to be in very similar conformations in those structures. Least-squares superposition was therefore applied to these main chain atoms. The resulting overlapped structures showed significant differences in their acyl- or aryl-binding pockets (Figure 2B). Consistent with the highest sequence similarity between BcDltA and PheA (29% identity), the two structures showed the highest similarity in main chain conformations of residues lining up the amino acid-

binding pocket (cyan and magenta, respectively, Figure 2B). Equivalent to Asp-177 of BcDltA, Asp-235 of PheA stabilizes the amino group of the substrate. Nearby, Ile-330 of PheA and the equivalent Val-301 of BcDltA both have an unusual conformation in the disfavored region on a Ramachandran plot. Consistent with the requirement for binding a bulkier phenylalanine substrate, PheA has smaller side chains at Ala-236 (Leu-178 of BcDltA) and Ala-301 (Cys-269 of BcDltA). The DhbE and yeast ACS structures (green and yellow, respectively, Figure 2B) have drastically different dispositions of one of their respective aryl- or acyl-binding residues corresponding to Val-301 of BcDltA (cyan and labeled, Figure 2B).

D-Alanine Is the Preferred Substrate over L-Alanine. In order to analyze the likely preference for D-alanine over L-alanine, we studied the initial rates of the first-step reaction catalyzed by BcDltA by monitoring the pyrophosphatase-coupled release of inorganic phosphate. The initial rates of this reaction appeared to have reached a plateau in the presence of 5 mM D-alanine and 1 mM or higher concentrations of ATP (data not shown). The reaction rates were therefore measured in the presence of 5 mM ATP and varied concentrations of D- or L-alanine (Figure 3A). The curve of the reaction rates against alanine concentrations appeared to be hyperbolic, which is consistent with the protein being monomeric in gel filtration (data not shown) and in the crystal. The derived apparent dissociation constant (K_M) and turnover rates (k_{cat}) are listed in Table 2. For D-alanine, K_M was estimated as 1.1 ± 0.2 mM. For L-alanine, a noticeably larger dissociation constant was derived (14.4 ± 1.6 mM). The estimated turnover rate for D-alanine (1.5 ± 0.1 min^{-1}) was lower than that for L-alanine (6.7 ± 0.4 min^{-1}). In the presence of 2 mM or lower concentrations of alanine, the observed reaction rates for the D-form were significantly faster than those for the L-form at the same alanine concentration.

C269A Mutation Relaxes D-Alanine Preference. Cys-269 in the BcDltA structure has its side chain dispositioned in a way which would clash with the α-methyl group of an L-alanine. Mutation for a smaller Ala was made at this position. The purified C269A protein showed relaxed enantiomer selection as expected (Figure 3B). The apparent dissociation constant (K_M) for D-alanine was estimated as 3.1 ± 0.3 mM. For L-alanine, a larger dissociation constant was derived (6.6 ± 0.5 mM). The K_M gap was noticeably smaller than that of the wild-type protein (between 1.1 and 14.4 mM). The estimated turnover rates (k_{cat}) were 6.2 ± 0.2 min^{-1} for D-alanine and 7.6 ± 0.3 min^{-1} for L-alanine. Unlike the wild-type protein which showed a ~4-fold smaller k_{cat} value for D-alanine than that for L-alanine, the C269A mutant protein appeared to have very similar k_{cat} values for both enantiomers.

Sequence Alignment of Representative DltAs and PheA. The amino acid sequences of adenylation domains vary significantly. Even between the DltA proteins from Gram-positive bacteria, less that 60% sequence identities were found between DltA from *B. cereus* and those from model organism *B. subtilis* (56%) and pathogenic microbe *S. aureus* (43%), *Streptococcus pneumoniae* (42%), and *Clostridium difficile* (43%). BcDltA closely resembles DltA from *Bacillus anthracis* (501 out of 504 residues are identical) as expected from the fact that the two species are arguably one. In

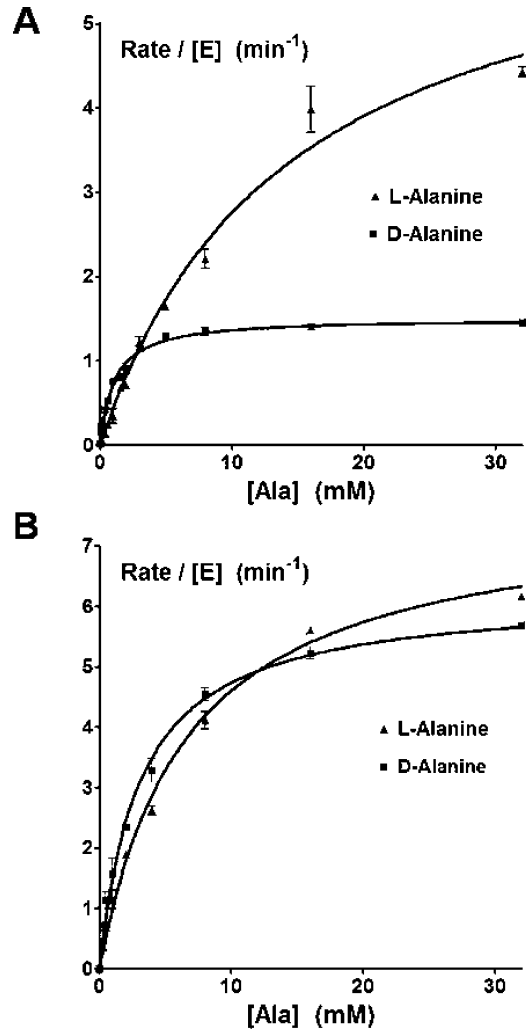

FIGURE 3: Rate of pyrophosphate release catalyzed by BcDltA in the presence of D- and L-alanine. The reaction solutions contained 0.005 mM wild-type or mutant BcDltA, 5 mM ATP, 0.1 M KCl, 0.01 M $MgCl_2$, 0.05 M Tris-HCl buffer at pH 7.4, 5 units/mL yeast inorganic pyrophosphatase (Sigma-Aldrich), and specified concentration of alanine (Sigma-Aldrich). The initial rates of pyrophosphate accumulation divided by the BcDltA concentration were shown. (A) Reaction catalyzed by the wild-type BcDltA. (B) Reaction catalyzed by the C269A mutant protein.

Table 2: Kinetic Data for DltA Protein from *B. cereus*

BcDltA (alanine)	K_M ($\times 10^{-3}$ M)	k_{cat} (min^{-1})	k_{cat}/K_M (mM$^{-1}\cdot$min^{-1})
wild type (D-Ala)	1.1 ± 0.2	1.5 ± 0.1	1.4 ± 0.2
wild type (L-Ala)	14.4 ± 1.6	6.7 ± 0.4	0.47 ± 0.05
C269A (D-Ala)	3.1 ± 0.3	6.2 ± 0.2	2.0 ± 0.2
C269A (L-Ala)	6.6 ± 0.5	7.6 ± 0.3	1.2 ± 0.1

contrast, BcDltA was found to share only 29% sequence identity with PheA, the closest homologue outside the DltA family. Sequence alignment (Figure 4) showed that the two proteins' amino acid-binding pockets are highly conserved. BcDltA's segment of Phe-196 to Leu-198 belongs to an invariable motif SFDLSV among the DltA representatives. In comparison, PheA has a similar SFDASV sequence (the equivalent residue of BcDltA's Leu-178 is substituted by an Ala). Similarly sized residues (Cys, Ile, Asp) were found in these DltAs at the position equivalent to Cys-269 of BcDltA. PheA has a smaller Ala at this position. The DltAs also share a N(T/A/G)YGPTEATV motif equivalent to residues from 292 to 301 of BcDltA. PheA is also similar in

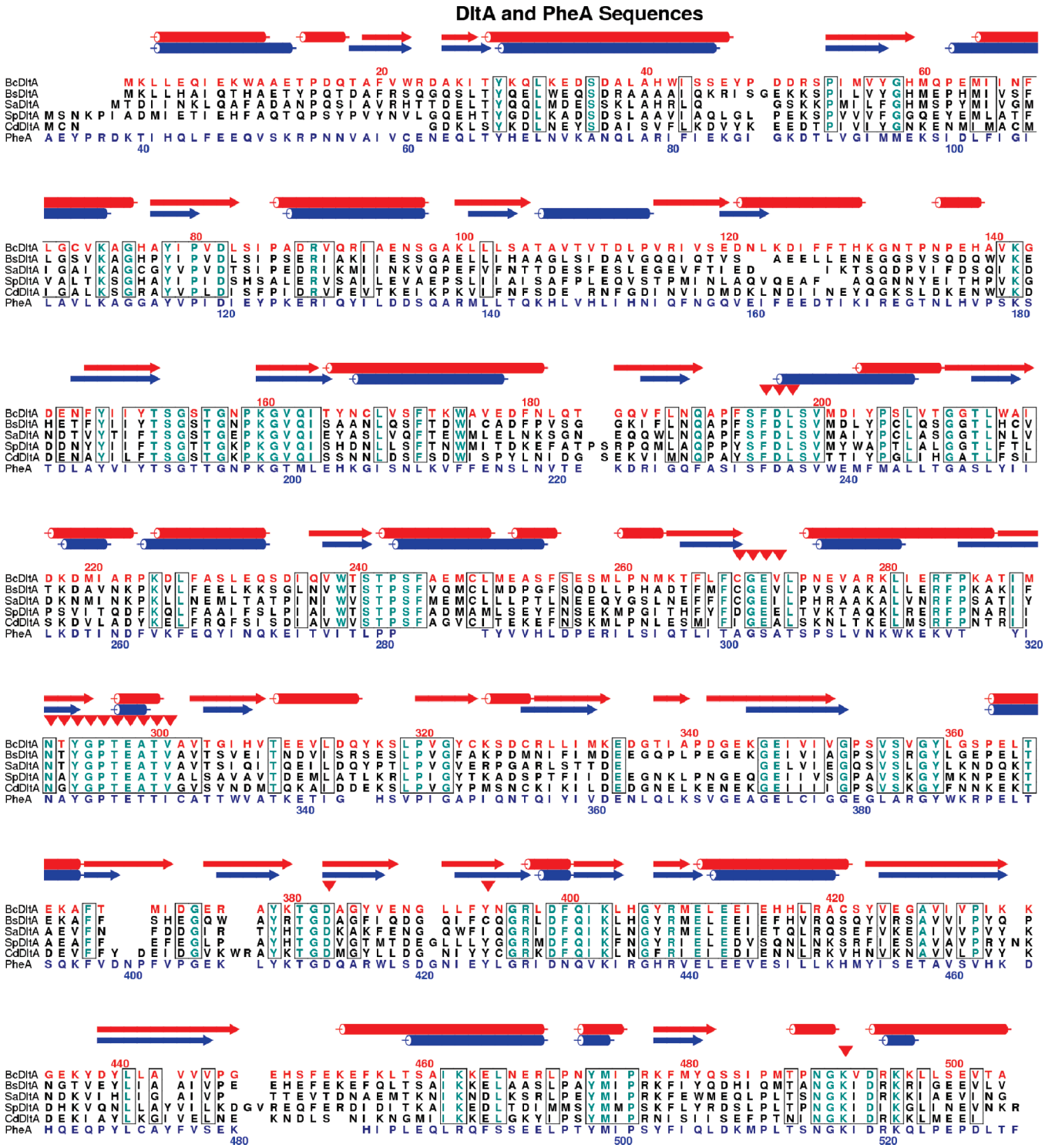

FIGURE 4: Sequence alignment of selected DltAs and PheA. Sequence alignment of DltA homologues from *B. cereus* (BcDltA), *B. subtilis* (BcDltA), *S. aureus* (SaDltA), *S. pneumoniae* (SpDltA), and *C. difficile* (CdDltA) and PheA domain from *B. brevis* gramicidin S synthetase I. The sequences were aligned by ClustalW (*38*). Sequences, secondary structures, and residue numbers of BcDltA and PheA were shown in red and blue, respectively. Invariable residues within the DltA family were highlighted in cyan. Highly conserved segments within the DltA family were boxed. The D-alanine adenylate-contacting residues in BcDltA were marked with arrows. This alignment figure is generated by Alscript (*39*).

this segment with a sequence of NAYGPTETTI with differences limited to the last and third last positions.

DISCUSSION

Bacteria selectively incorporate D-alanine in various cell wall components. In Gram-positive bacteria, there is no exception in the ubiquitous alanyl esterification of teichoic acids. The measured apparent dissociation constants for D- and L-alanine suggest that the bacterium favors the use of D-alanine. In cultured cells of *E. coli* and *B. subtilis*, a previous study (*37*) found that intracellular D-alanine (in the order of 10^2 μM) is approximately 20-fold more abundant than the L-enantiomer (in the order of 10^1 μM). As suggested by the apparent dissociation constants (~1.1 mM for

D-alanine and ~14 mM for L-alanine), BcDltA likely operates in a cellular environment where D- and L-alanine concentrations are significantly less than their respective K_M. As a result, the substrate concentrations and the enzyme's specificity constants (k_{cat}/K_M) would serve as indicators of substrate selectivity. Such specificity constants of BcDltA are 1.4 mM^{-1} min^{-1} for D-alanine, and 0.47 mM^{-1} min^{-1} for L-alanine. In combination with a possible 20-fold difference in D- and L-alanine concentration, BcDltA would favor D- over L-alanine by approximately 60-fold. In nonribosomal peptide synthesis, adenylation domains such as PheA function as a complex with peptide carrier domains. It is possible that DltA may achieve higher selectivity in a complex with DltC. Interestingly, the turnover rate for D-alanine is ~4-fold smaller than that of L-alanine in the adenylation reaction. Although our data do not provide an experimental explanation, the slower rate may be caused by slower release of the D-alanine adenylate. This assumption is consistent with the structural finding that the binding pocket is perfect for D-alanine but not L-alanine due to the disposition of the Cys-269 side chain. A slower release rate would be clearly advantageous for retention of the adenylate and subsequent transfer of the D-alanyl group to the thiol acceptor on DltC. Usually in nonribosomal peptide synthesis, L-amino acids are activated by adenylation domains and sometimes racemized by epimerization domains for subsequent conversion into the D-form (*11*). There is no such epimerization domain known to associate with D-alanylation of teichoic acid. The DltA protein from Gram-positive bacteria may therefore stand out as the first structurally characterized adenylation domain that selectively activates a D-amino acid.

Similarity in primary sequences as well as in tertiary structures between BcDltA and PheA suggests that the D-alanine-activating DltA proteins and the phenylalanine-activating domain PheA in nonribosomal peptide synthesis may have evolved from a common ancestor. Our results suggest that the preference for D-alanine is partly determined by steric hindrance imposed by the side chain of Cys-269 on L-alanine but not D-alanine. Despite lower than 60% sequence identity between representative DltA proteins, their D-alanine specific binding pocket appears to be highly conserved. It is therefore possible to design a common inhibitor for combating infectious diseases caused by Gram-positive bacteria. The crystal structure of BcDltA outlined structural similarities among adenylation domains as well as differences in their respective acyl- or aryl-recognition pocket. The differences would aid in the design of DltA-specific inhibitors without impeding the normal functions of similar human enzymes such as the ubiquitous acetyl-CoA synthetase.

ACKNOWLEDGMENT

We thank Drs. Gabriele Schatte and Wilson Quail for assistance with the X-ray facility at the Saskatchewan Structural Sciences Centre. We also thank Dr. Stanley Moore for helpful discussions and comments on the manuscript.

REFERENCES

1. Armstrong, J. J., Baddiley, J., Buchanan, J. G., Davision, A. L., Kelemen, M. V., and Neuhaus, F. C. (1959) Composition of teichoic acids from a number of bacterial walls. *Nature 184*, 247–248.
2. Hyyrylainen, H. L., Vitikainen, M., Thwaite, J., Wu, H., Sarvas, M., Harwood, C. R., Kontinen, V. P., and Stephenson, K. (2000) D-Alanine substitution of teichoic acids as a modulator of protein folding and stability at the cytoplasmic membrane/cell wall interface of Bacillus subtilis. *J. Biol. Chem. 275*, 26696–26703.
3. Fischer, W. (1988) Physiology of lipoteichoic acids in bacteria. *Adv. Microb. Physiol. 29*, 233–302.
4. Perego, M., Glaser, P., Minutello, A., Strauch, M. A., Leopold, K., and Fischer, W. (1995) Incorporation of D-alanine into lipoteichoic acid and wall teichoic acid in Bacillus subtilis. Identification of genes and regulation. *J. Biol. Chem. 270*, 15598–15606.
5. Neuhaus, F. C., and Baddiley, J. (2003) A continuum of anionic charge: structures and functions of D-alanyl-teichoic acids in gram-positive bacteria. *Microbiol. Mol. Biol. Rev. 67*, 686–723.
6. Wecke, J., Perego, M., and Fischer, W. (1996) D-alanine deprivation of Bacillus subtilis teichoic acids is without effect on cell growth and morphology but affects the autolytic activity. *Microb. Drug Resist. 2*, 123–129.
7. Peschel, A., Otto, M., Jack, R. W., Kalbacher, H., Jung, G., and Gotz, F. (1999) Inactivation of the dlt operon in Staphylococcus aureus confers sensitivity to defensins, protegrins, and other antimicrobial peptides. *J. Biol. Chem. 274*, 8405–8410.
8. Kristian, S. A., Lauth, X., Nizet, V., Goetz, F., Neumeister, B., Peschel, A., and Landmann, R. (2003) Alanylation of teichoic acids protects Staphylococcus aureus against Toll-like receptor 2-dependent host defense in a mouse tissue cage infection model. *J. Infect. Dis. 188*, 414–423.
9. Gross, M., Cramton, S. E., Gotz, F., and Peschel, A. (2001) Key role of teichoic acid net charge in Staphylococcus aureus colonization of artificial surfaces. *Infect. Immun. 69*, 3423–3426.
10. Gotz, F. (2002) Staphylococcus and biofilms. *Mol. Microbiol. 43*, 1367–1378.
11. Stachelhaus, T., Mootz, H. D., and Marahiel, M. A. (1999) The specificity-conferring code of adenylation domains in nonribosomal peptide synthetases. *Chem. Biol. 6*, 493–505.
12. Conti, E., Franks, N. P., and Brick, P. (1996) Crystal structure of firefly luciferase throws light on a superfamily of adenylate-forming enzymes. *Structure 4*, 287–298.
13. Debabov, D. V., Kiriukhin, M. Y., and Neuhaus, F. C. (2000) Biosynthesis of lipoteichoic acid in Lactobacillus rhamnosus: role of DltD in D-alanylation. *J. Bacteriol. 182*, 2855–2864.
14. May, J. J., Finking, R., Wiegeshoff, F., Weber, T. T., Bandur, N., Koert, U., and Marahiel, M. A. (2005) Inhibition of the D-alanine: D-alanyl carrier protein ligase from Bacillus subtilis increases the bacterium's susceptibility to antibiotics that target the cell wall. *FEBS J. 272*, 2993–3003.
15. Zheng, L., Baumann, U., and Reymond, J. L. (2004) An efficient one-step site-directed and site-saturation mutagenesis protocol. *Nucleic Acids Res. 32*, e115.
16. Wu, Y., He, Y., Moya, I. A., Qian, X., and Luo, Y. (2004) Crystal structure of archaeal recombinase RadA; A snapshot of its extended conformation. *Mol. Cell 15*, 423–435.
17. Conti, E., Stachelhaus, T., Marahiel, M. A., and Brick, P. (1997) Structural basis for the activation of phenylalanine in the nonribosomal biosynthesis of gramicidin S. *EMBO J. 16*, 4174–4183.
18. Bernstein, F. C., Koetzle, T. F., Williams, G. J., Meyer, E. F., Jr., Brice, M. D., Rodgers, J. R., Kennard, O., Shimanouchi, T., and Tasumi, M. (1977) The Protein Data Bank. A computer-based archival file for macromolecular structures. *Eur. J. Biochem. 80*, 319–324.
19. Berman, H., Henrick, K., and Nakamura, H. (2003) Announcing the worldwide Protein Data Bank. *Nat. Struct. Biol. 10*, 980.
20. Navaza, J. (2001) Implementation of molecular replacement in AMoRe. *Acta Crystallogr., Sect. D: Biol. Crystallogr. 57*, 1367–1372.
21. Perrakis, A., Morris, R., and Lamzin, V. S. (1999) Automated protein model building combined with iterative structure refinement. *Nat. Struct. Biol. 6*, 458–463.
22. McRee, D. E. (1999) XtalView/Xfit—A versatile program for manipulating atomic coordinates and electron density. *J. Struct. Biol. 125*, 156–165.

23. Brunger, A. T., Adams, P. D., Clore, G. M., DeLano, W. L., Gros, P., Grosse-Kunstleve, R. W., Jiang, J. S., Kuszewski, J., Nilges, M., Pannu, N. S., Read, R. J., Rice, L. M., Simonson, T., and Warren, G. L. (1998) Crystallography & NMR system: A new software suite for macromolecular structure determination. *Acta Crystallogr., Sect. D: Biol. Crystallogr. 54*, 905–921.
24. Kraulis, P. (1991) MOLSCRIPT: a program to produce both detailed and schematic plots of protein structures. *J. Appl. Crystallogr. 24*, 946–950.
25. Bacon, D. J., and Anderson, W. F. (1988) A fast algorithm for rendering space-filling molecule pictures. *J. Mol. Graphics 6*, 219–220.
26. Itaya, K., and Ui, M. (1966) A new micromethod for the colorimetric determination of inorganic phosphate. *Clin. Chim. Acta 14*, 361–366.
27. Chang, K. H., Xiang, H., and Dunaway-Mariano, D. (1997) Acyl-adenylate motif of the acyl-adenylate/thioester-forming enzyme superfamily: a site-directed mutagenesis study with the Pseudomonas sp. strain CBS3 4-chlorobenzoate:coenzyme A ligase. *Biochemistry 36*, 15650–15659.
28. Stuible, H., Buttner, D., Ehlting, J., Hahlbrock, K., and Kombrink, E. (2000) Mutational analysis of 4-coumarate:CoA ligase identifies functionally important amino acids and verifies its close relationship to other adenylate-forming enzymes. *FEBS Lett. 467*, 117–122.
29. Horswill, A. R., and Escalante-Semerena, J. C. (2002) Characterization of the propionyl-CoA synthetase (PrpE) enzyme of Salmonella enterica: residue Lys592 is required for propionyl-AMP synthesis. *Biochemistry 41*, 2379–2387.
30. Walker, J. E., Saraste, M., Runswick, M. J., and Gay, N. J. (1982) Distantly related sequences in the alpha- and beta-subunits of ATP synthase, myosin, kinases and other ATP-requiring enzymes and a common nucleotide binding fold. *EMBO J. 1*, 945–951.
31. Gulick, A. M., Starai, V. J., Horswill, A. R., Homick, K. M., and Escalante-Semerena, J. C. (2003) The 1.75 Å crystal structure of acetyl-CoA synthetase bound to adenosine-5′-propylphosphate and coenzyme A. *Biochemistry 42*, 2866–2873.
32. Reger, A. S., Carney, J. M., and Gulick, A. M. (2007) Biochemical and crystallographic analysis of substrate binding and conformational changes in acetyl-CoA synthetase. *Biochemistry 46*, 6536–6546.
33. Laskowski, R. A., Watson, J. D., and Thornton, J. M. (2005) ProFunc: a server for predicting protein function from 3D structure. *Nucleic Acids Res. 33*, W89−93.
34. Linne, U., Schafer, A., Stubbs, M. T., and Marahiel, M. A. (2007) Aminoacyl-coenzyme A synthesis catalyzed by adenylation domains. *FEBS Lett. 581*, 905–910.
35. May, J. J., Kessler, N., Marahiel, M. A., and Stubbs, M. T. (2002) Crystal structure of DhbE, an archetype for aryl acid activating domains of modular nonribosomal peptide synthetases. *Proc. Natl. Acad. Sci. U.S.A. 99*, 12120–12125.
36. Jogl, G., and Tong, L. (2004) Crystal structure of yeast acetyl-coenzyme A synthetase in complex with AMP. *Biochemistry 43*, 1425–1431.
37. Manning, J. M., Merrifield, N. E., Jones, W. M., and Gotschlich, E. C. (1974) Inhibition of bacterial growth by beta-chloro-D-alanine. *Proc. Natl. Acad. Sci. U.S.A. 71*, 417–421.
38. Pearson, W. R., and Lipman, D. J. (1988) Improved tools for biological sequence comparison. *Proc. Natl. Acad. Sci. U.S.A. 85*, 2444–2448.
39. Barton, G. J. (1993) ALSCRIPT: a tool to format multiple sequence alignments. *Protein Eng. 6*, 37–40.

BI801363B